PCCP

PAPER

View Article Online
View Journal | View Issue

Published on 16 August 2016. Downloaded by UNIVERSIDAD SAO PAULO on 21/10/2016 16:36:44.

Cite this: *Phys. Chem. Chem. Phys.*, 2016, **18**, 25582

How do random superficial defects influence the electro-oxidation of glycerol on Pt(111) surfaces?†

Pablo S. Fernández,*[a] Polina Tereshchuk,[b] Camilo A. Angelucci,[c] Janaina F. Gomes,[d] Amanda C. Garcia,[b] Cauê A. Martins,[e] Giuseppe A. Camara,[f] María E. Martins,[g] Juarez L. F. Da Silva[b] and Germano Tremiliosi-Filho[b]

Received 8th July 2016,
Accepted 16th August 2016

DOI: 10.1039/c6cp04768h

www.rsc.org/pccp

The glycerol electrooxidation reaction (GEOR) has attracted huge interest in the last decade due to the very low price and availability of this polyol. In this work, we studied the GEOR on Pt(111) electrodes by introducing different densities of random defects. Our results showed that the generation of defects on Pt(111) slightly modified the GEOR onset potential, however it generates changes in the voltammetric oxidation charges and also in the relative production of CO_2 to carbonyl containing compounds, C=O. The voltammetric profiles in the forward scan show two oxidation peaks. FTIR data show that the first one is connected with the GlOH dissociative adsorption to form CO (and others intermediates) while the second one, at higher potentials, matches the onsets of the CO oxidation to CO_2 and the C=O production. FTIR also confirms that the lower activity of defected electrodes at lower potentials is connected to a higher CO poisoning. DFT calculations show that the presence of CO molecules on a Pt defected surface keeps water and GlOH molecules far from the surface and linked by H bonds. This paper is the last of a series of three works where we explore the GEOR on an important number of different Pt surfaces. These works show that it is difficult to oxidize GlOH at potentials lower than 0.6 V (under our experimental conditions) without suffering an important electrode poisoning (mainly by CO). Since the structure of nanoparticles might be mimicked by defected single crystals, these sets of reports provide a considerable amount of information concerning the influence of such surfaces towards GlOH reaction in acidic media. Therefore, if the well-known "nano"-effect does not produce substantial changes in the activity of Pt materials, they are not useful to be applied in a Direct Glycerol Fuel Cell (DGFC). On the other hand, it is very interesting that the density of electrode defects permits us to tune the relative production of CO_2 to C=O.

1 Introduction

The discussion about the global energy demand is a subject that became a general concern of the most industrialized governments in the last few decades.[1] The conversion of biomass products into chemicals and/or fuels is considered a green alternative to similar petroleum processes. Biodiesel production from transesterification of vegetable oils and animal fats is one important process in this scenario, which is increasing year by year. However, from this specific chemical process, concomitant to biodiesel yielding, crude glycerol (GlOH) is obtained on a proportion of 10 : 1 (biodiesel : GlOH). Nowadays, due to the expansion of biodiesel consumption the amount of GlOH supply in the global market has become greater than commercial demand, causing a drop in prices.[2] Such a low valuable feedstock justifies the development of new processes focusing on the conversion of glycerol into fine chemicals.

In this context electrocatalysis provide a potential alternative to produce compounds with high value as dihydroxyacetone,

[a] *Chemistry Institute, State University of Campinas, PO Box 6154, 13083-970, Campinas SP, Brazil. E-mail: pablo.fernandez@iqm.unicamp.br*
[b] *São Carlos Institute of Chemistry, University of São Paulo, PO Box 780, 13560-970, São Carlos, SP, Brazil*
[c] *Center of Natural and Human Sciences, Federal University of ABC, Av. dos Estados, 5001, Santo André, Brazil*
[d] *Chemical Engineering Department, Federal University of São Carlos, P.O. Box 676, 13565-905, São Carlos, SP, Brazil*
[e] *Faculty of Exact Sciences and Technology, Federal University of Grande Dourados, 79804-970, Dourados, MS, Brazil*
[f] *Institute of Chemistry, Universidade Federal de Mato Grosso do Sul, C.P. 549, 79070-900, Campo Grande, MS, Brazil*
[g] *Physical Chemistry Research Institute (INIFTA), Exact Sciences Faculty, CCT La Plata-CONICET, C.P. 1900, La Plata, Argentina*

† Electronic supplementary information (ESI) available: (i) Details about the generation of defects and the CVg in the presence of GlOH for all the electrodes studied here; (ii) a comparison of the FTIR spectra obtained with the same surfaces and ATR spectra of some GlOH oxidation products and (iii) detailed information about all the systems studied by DFT. We also include two sections entitled: "The role of the vdW interaction" and "The work function change". See DOI: 10.1039/c6cp04768h

 This journal is © the Owner Societies 2016

Published on 16 August 2016. Downloaded by UNIVERSIDAD SAO PAULO on 21/10/2016 16:36:44.

glyceraldehyde, among others.[3–10] The range of products formed from GlOH oxidation is highly dependent on catalyst composition,[3–10] pH,[8,11] crystallographic orientation of the atoms on the catalyst surface,[10–14] *etc.*

The structure sensitivity of glycerol electrooxidation reaction (GEOR) follows the trend of the oxidation of small organic molecules on platinum. It has been shown that different Pt single crystal surfaces lead to different electrocatalytic activities towards the GEOR. Recently, Garcia *et al.* showed that Pt(100) surfaces selectively oxidize the terminal carbon of GlOH producing only glyceraldehyde (Gld). On the other hand, both the secondary and primary carbons can be oxidized over Pt(111) to generate Gld and dihydroxyacetone (DHA).[10]

In previous works,[12,13] we showed that the use of well-ordered single crystal electrodes provided the first insights into how diluted surface defects influence GEOR. Starting from Pt(100) surfaces free of defects, our results indicate that as random defects are added, the surfaces become increasingly poisoned by CO produced during the GEOR, the binding energy of which increases with the defect density. Although these results were obtained from fundamental studies with single crystal electrodes, they help to shed some light on the desirable characteristics of a surface, ultimately aiming to design nanoparticles, the crystallographic orientations of which allow the guidance of electrochemical reactions towards specific pathways.

In a similar strategy, but using Pt nanoparticles with (111) and (100) preferentially oriented surfaces, Buso-Rogero *et al.*[15] recently reported that the mechanism of ethanol electrooxidation depends on the surface structure; namely, those reaction pathways that require a C–C bond cleavage to occur preferentially on (100) domains. On the other hand, Aran-Ais *et al.* by studying the electrooxidation of ethylene glycol (EG) found that on the Pt(111) surface the C–C bond is readily broken, with higher activity when diluted (110) orientation defects were present.[16] The authors stressed out how the presence of a vicinal alcohol group in the EG molecule structure facilitates the C–C bond cleavage at low potentials when compared with ethanol electrooxidation reaction. These results are in line with the other results we previously reported for GlOH on polycrystalline Pt.[17]

With the aim of understanding the surface structure sensitivity of GEOR we prepared several Pt(111) surfaces with different degrees of defects and studied the GEOR using Cyclic Voltammetry (CV) and FTIR *in situ*. We show that the reaction is very sensitive to the modification of the surfaces during the first scan. The stable CV (obtained after about 10 cycles) also changes, but to a lower extent, with the electrochemical behaviour being dominated by CO poisoning. This result was confirmed by FTIR experiments. To address the atomistic structure of the systems and the interaction of molecules with substrates, we performed DFT calculations, which help to understand the experimental results. We obtained the atomic level structure of the mixture of water, GlOH (as the most important molecules of our system), and CO (which is the only adsorbed reaction intermediate detected till now) on the defected Pt surface. We showed that water and GlOH are not able to displace CO molecules adsorbed on Pt sites, even when Pt–CO bindings are weakened by the repulsive forces caused by high CO coverage. Furthermore, we calculated the work function change, which is useful in the atomic level understanding of the interaction between the molecules and the defected surface, *i.e.* it gives information about the direction of an effective charge transfer, a possible charge transfer or the polarization effects.

Interestingly, we find a different trend in the C=O/CO_2 ratio (measured using the FTIR band intensities) for Pt(100) and Pt(111) defected surfaces. For Pt(100) the C=O/CO_2 ratio augments with the defect density, which is very likely due to an increase in the relative production of glyceric acid (GA). On the other hand, the decrease of the C=O/CO_2 ratio with the defect density of Pt(111) surfaces is probably due to a decrease in the relative production of DHA.

We will compare the results of this work with those obtained with defected Pt(100) surfaces and with the recent work of Garcia *et al.*[10] However, it is worth noting that the conditions used in that paper (0.1 M GlOH + 0.5 M $HClO_4$)[10] are different from ours (0.2 M of GlOH + 0.5 M of H_2SO_4).

2 Experimental section

2.1 Electrochemical systems and spectroelectrochemical experiments

All experiments were performed at room temperature (25 ± 1 °C) in a conventional three-electrode electrochemical cell. A high-area polycrystalline Pt sheet was used as a counter electrode. The reference electrode was a reversible hydrogen electrode (RHE). The working electrode was a 1 cm diameter Pt(111) disc acquired from SPL company (Surface Preparation Laboratory).

The FTIR instrument was a Bruker Vertex 80V IR spectrometer equipped with a liquid nitrogen cooled detector. Spectra were computed from an average of 128 interferograms. The spectral resolution was set to 4 cm^{-1}. First, the working electrode was placed in the meniscus configuration, and five consecutive cyclic voltammograms (CVgs) were obtained in a solution of 0.2 M GlOH and 0.5 M of H_2SO_4. The potential was maintained at 0.10 V, and the electrode was dipped in the solution until it came into contact with the window. When the system became stable (the recorded spectra did not change with time at 0.10 V), potential steps of 0.05 V were applied between 0.10 V and 0.95 V, holding each potential for enough time to obtain 128 interferograms (approximately 1 min). The first spectrum was obtained at 0.10 V and served as a reference, and then the potential was set at 0.15 V to record a new spectrum, and so on until 0.95 V.

2.2 Working electrode surface preparation

An ordered and clean Pt(111) surface was obtained by flame annealing the electrode in a butane–oxygen flame for 1 min followed by cooling it in a reductive H_2 : Ar ($\sim 1:3$) atmosphere for 3 min. The electrode surface was then protected with a water droplet saturated with cooling gases to prevent contamination and reconstruction of the surfaces during the transfer to the electrochemical cell.

Published on 16 August 2016. Downloaded by UNIVERSIDAD SAO PAULO on 21/10/2016 16:36:44.

To monitor the influence of the upper potential limit on the Pt(111) surface order degree, the potential limit was progressively augmented from 0.9 V until 1.3 V. Through this experiment we determined that: (i) Pt(111) surfaces cycled until 1.1 V remain unchanged and well ordered (at least for some cycles) and (ii) cycling up to 1.3 V generates a progressive disorder on the surface, which gives the possibility of aborting the experiments after generating the desired density of defects.

In this work, we prepare electrodes with four different defect degrees. These surfaces will be labelled as "Pt(111)-*X*", where "*X*" indicates the number of cycles between 0.05 V and 1.30 V performed to generate the defects on the Pt(111) surface.

After performing the protocol to generate defects, the surface order was checked again by recording CVgs in the potential range between 0.05 V and 0.90 V in a 0.5 M H_2SO_4 solution. Then, the disc was protected by a solution droplet and transferred to an identical electrochemical cell containing a 0.5 M H_2SO_4 and 0.2 M GlOH solution to study the GEOR. The electrode was placed in contact with the solution at 0.12 V in all experiments. This potential was chosen to minimize faradaic processes other than GlOH dissociative adsorption.[18] The GEOR CV experiments were performed in the potential range between 0.05 V and 0.95 V.

2.3 Theoretical approach and computational details

Total energy calculations were performed using DFT within the generalized gradient approximation proposed by Perdew–Burke–Ernzerhof (PBE).[19] To improve the description of the long range van der Waals (vdW) interactions, we employed the DFT-D3 approach proposed by S. Grimme,[20] in which two- and three-body terms are taken into account. The Kohn–Sham equations were solved using the all-electron projected augmented wave (PAW) method[21,22] and the PAW projectors to describe electron–ion interactions as implemented in the Vienna *Ab Initio* Simulation Package (VASP).[23,24] The total energy calculations were performed using a plane-wave cut-off energy of 487 eV, while a $3 \times 3 \times 1$ *k*-point mesh was employed for the surface calculations for the integration of the Brillouin zone.

To model the Pt(111) surface, the repeated slab geometry was used with five layers, a (4×4) surface unit cell and 26 Å for the vacuum region. The defected Pt(111) surface was constructed by removing 10 surface atoms, and, hence, the remaining 6 atoms on the surface are lower coordinated, Pt_6. Moreover, we also removed one atom from the second layer. Thus, the defected surface consists of a topmost layer with 6 Pt atoms, Pt_6, a second layer with 15 atoms, Pt_{15}, and subsequent layers consisting of 16 atoms approaching the bulk-like structure. Thus, our substrate is called $Pt_6/Pt_{15}/Pt(111)$. The adsorbed molecules were placed only on one side of the slab, and hence, we employed the dipole correction for the total energy and work function calculations. For all calculations only the bottom layer of the slab was frozen, while other four layers and the adsorbates were allowed to relax.

2.4 Generation of atomic configurations

To obtain reliable adsorbed configurations on $Pt_6/Pt_{15}/Pt(111)$, we performed the following steps:

(i) Several initial configurations are based on the single GlOH, water, and CO molecules on the different locations of the defected Pt(111) substrate.

(ii) The initial configurations of 2 GlOH molecules on the surface were built up taking into account different molecular locations: (a) 2 GlOH molecules are on the Pt_6 defects forming H bonds; (b) 1 GlOH is on the Pt_6 defects and 1 GlOH is on the terrace; (c) only 1 GlOH is on the defect forming a H bond with another GlOH not attached to the surface; (d) 1 GlOH is on the defect and 1 GlOH is on the terrace surface creating a H bond; (e) 2 GlOH molecules are on the terrace forming a H bond between them and (f) 2 separate GlOH molecules are on the terrace.

(iii) For 12 water molecules, we modelled the following systems: (a) only 2 water molecules are on the terrace, the others are farther, creating H bonds; (b) 1 water is on the terrace and 1 water molecule is on the defect, the remaining ones are farther from the surface forming H bonds; (c) all of the molecules are far from the surface and 9 of them create H bonds; (d) all molecules bind with Pt atoms of the surface and create H bonds; (e) 2 molecules are on the defects, the rest is farther and 9 of them create H bonds; and (f) 2 molecules are on the defect, and 2 are on the terrace (one is close to the vacancy), the others are farther and all the molecules are bound through H.

(iv) For 6 CO molecules on the surface, initial configurations present the structures in which molecules are on-top, bridge and hollow sites and located on the defects, terraces or vacant places.

(v) Finally, several initial configurations for the mixture of 2 GlOH, 12 water and 6 CO molecules on the surface were built up. A few of them were based on the optimized structures of 2 GlOH and 6 CO molecules on the substrate, while others were modelled intuitively, by manipulating different locations and distances from the surface. Moreover, to obtain more precise structures of the mixture of 2 GlOH, 12 water and 6 CO molecules on the surface we applied molecular dynamics (MD) simulations started at 100 K and decreased up to 0 K, from which a few snapshots (around 5) at every 1000 steps were chosen for further optimization. The equilibrium geometries were achieved once the atomic forces were smaller than 0.05 eV $Å^{-1}$ on each atom, with a total energy convergence of 10^{-6} eV. Most of the optimized structures along with their relative total energies are given in figures in the ESI.†

Analysis. To get a deeper understanding of the interaction strength of the molecules with the defected Pt surfaces, we calculated adsorption energy as $E_{ad} = E^{Molecule/Pt} - (n \times E^{Molecule} + E^{clean\ Pt})$, where $E^{Molecule/Pt}$, $E^{Molecule}$ and $E^{clean\ Pt}$ are the total energies of the system with n molecules, a molecule in the gas-phase, and the clean Pt surface, respectively. Additionally, to achieve a deeper comprehension of the interaction mechanism, we performed additional calculations and analysis of the work function change, $\Delta\Phi = \Phi^{Molecules/Pt} - \Phi^{clean\ Pt}$, where $\Phi^{molecules/Pt}$ and $\Phi^{clean\ Pt}$ are work functions of molecules on the defected Pt(111) surfaces and the clean defected Pt(111) surface, respectively. The analysis of the work function change is useful in the identification of the direction of an effective charge transfer, a possible charge transfer or the polarization effects.

 This journal is © the Owner Societies 2016

Published on 16 August 2016. Downloaded by UNIVERSIDAD SAO PAULO on 21/10/2016 16:36:44.

3 Results and discussion

3.1 Pt(111) modified electrode characterization

As an introduction to GEOR results on the Pt(111) surface, it is mandatory to analyse carefully the CV profiles in the absence of GlOH, since the alcohol oxidation is highly dependent on the surface orientation.[12,14]

The Pt(111) CVg in acidic media is well understood, and can provide useful information to characterize the symmetry and distribution of surface sites,[25–27] as well as the system's general conditions and cleanliness.[25–27] Therefore, our starting point is the well-ordered Pt(111) voltammogram obtained after the flame annealing (black curve displayed in Fig. 1). The overall profile is in agreement with previous works,[25,28] showing a flat current plateau between 0.07 V and 0.30 V, assigned to hydrogen desorption reaction, followed by (bi)sulfate desorption, characterized by a hump and a spike that appear at 0.35 V and 0.42 V, respectively. In particular, the so-called hydrogen adsorption/desorption region is very useful for qualitative as well as quantitative characterization of Pt surfaces, since the voltammetric features of Pt in H_2SO_4 solution are highly sensitive to the surface structure.

In order to achieve different but systematic surface electrode configurations, we applied successive potential cycles on the well-ordered Pt(111) electrode up to 1.30 V, maintaining the lower potential at 0.05 V. The excursion in potentials where the oxygen adsorption takes place (>1.15 V) causes irreversible surface structural modifications.[25,29,30] Such modifications on a well ordered surface can be assigned to single ad-atoms, small islands, pits or other collections of defects, as described by Feliu's group publications through electrochemical experiments and Watanabe's group using STM.[25,27]

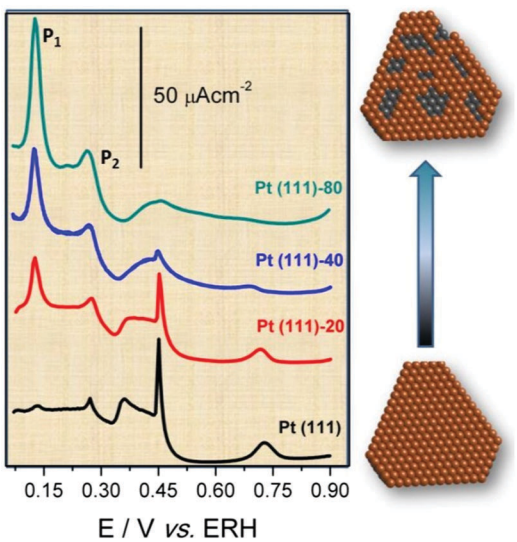

Fig. 1 Blank voltammograms' forward scans obtained in 0.5 M H_2SO_4 solution with four different degrees of defects on Pt(111) surfaces. The black voltammogram (bottom) shows the typical electrochemical response of a well-ordered (111) surface. Cycling up to 1.30 V generates defective electrode surfaces. The number of defects increases progressively from bottom up.

Thus, the surface changes provoked by continuous cycling is manifested as significant changes on the Pt(111) CVg (see Fig. S1, ESI†). In the hydrogen region, two reversible peaks can be observed: at 0.12 V and 0.27 V, labelled as P_1 and P_2, respectively. P_1 becomes wider and higher whereas P_2 reaches a maximum and shifts towards lower potentials. The adsorption states, P_1 and P_2, can be straightforward connected to the presence of defect sites (steps and kinks) with different geometries on the ordered Pt(111) surface. It can be done by comparison between the P_1 and P_2 features and those of Pt stepped electrodes which contain systematic defects on wide terraces. Such a comparison allows us to infer that the signal located at 0.12 V corresponds to defects with symmetries (110) while the peak at 0.27 V seems to correspond to defects with symmetry (100). However, all the defects generated on a (111) surface (ad-atoms, small islands, pits, *etc.*) are less stable than (110) sites, and some of these defects convert to (110) sites during cycling.[25]

The growing of defects on a surface clearly leads to a decrease of terrace domains. This behaviour can be noted in the anion adsorption region (>0.30 V) which is strongly dependent of the terrace size. The continuous cycling leads to a decrease of the adsorption charge which is a consequence of the fact that the terrace sites with (111) domains become smaller.

The result of using multiple cycles to change the surface by adding defects on a well ordered surface is illustrated for some representative cycles in Fig. 1. The curves are the forward scans of the stable voltammograms obtained by limiting the upper potential at 0.90 V.

In general, the CVg of disordered Pt(111)-*X* electrodes indicates that the surface retains the (111) symmetry, but there is a depletion of large domain widths while the defects increase with the number of incursions into the oxygen adsorption region.

Regarding the nature of the defects, Björling *et al.*[25] using a similar method for surface modification suggested from the symmetry and the intensity of P_1 that the defects formed during the modification are less ordered than mono-dimensional step sites, as those present on well-ordered stepped surfaces.

Summarizing, as was stated in our previous work,[13] it must be clear that although the CV responses of our surfaces are quite similar to those of Pt stepped model surfaces, the features of both structures are essentially different. The surfaces resulting from the application of multiple cycles present a random distribution of terraces and defected regions, the characteristics of which vary along the entire surface.[25,28]

Fig. S1 (ESI†) shows the electrochemical preparation of Pt(111)-80. After ending the cycling process, *i.e.* after attaining the 80th cycle, the potential limit was set again between 0.05 and 0.90 V to obtain the blank voltammogram shown in Fig. 1. To prepare Pt(111)-20, for instance, the cycling procedure of Fig. S1 (ESI†) was stopped in the 20th cycle and after that, the corresponding blank voltammogram was obtained between 0.05 and 0.90 V (Pt(111)-20 in Fig. 1).

3.2 GlOH electrooxidation on Pt(111) surfaces

Fig. S2 (ESI†) shows consecutive CVgs for all the surfaces studied. The CV features for GEOR change progressively from

Published on 16 August 2016. Downloaded by UNIVERSIDAD SAO PAULO on 21/10/2016 16:36:44.

the well-ordered surface, Pt(111), to the totally disturbed one, Pt(111)-80. For the sake of clarity, Fig. 2 shows only the first and the 20th CVg for each electrode.

As usual, the CV response is completely different in the first scan and tends to a characteristic profile along cycling. Fig. S3 (ESI†) compares the first and the characteristic cycle for all surfaces investigated. The first cycle is extremely sensitive to the arrangement of atoms on the surface. On the other hand, as the surfaces are cycled, the profile of the CVs tends to be uniform, regardless of their initial condition. Furthermore, Fig. 2 and Fig. S2 (ESI†) show a huge loss of activity for all the surfaces from the first to the characteristic cycle. In the positive going potential scan, all electrodes present two well-defined peaks. The first one centered at ~0.56 V is a broad peak that decreases significantly during cycling. In contrast, the second peak (a sharper, more developed peak located at ~0.78 V) is barely affected by the electrochemical cycling. By comparing the responses of Fig. S2 (ESI†), we conclude that they progressively change the behaviour from that of a Pt(111) single crystal surface to that of Pt(111)-80, tending to the response of Pt(110).[12] This behaviour is different from that observed with Pt(100)[13] where the introduction of defects does not affect considerably the current densities but generate a peak displacement towards more positive potentials. Besides, the shape of the CVg in the presence of GlOH is rather similar for electrodes with different densities of defects. Additionally, in contrast to that observed with Pt(111) surfaces, the most defected Pt(100) surface showed a behaviour completely different from that of a polycrystalline or a Pt(110) electrode.

Another important aspect of the CVs is the hysteresis between positive and negative scans. This phenomenon was reported to be intrinsically related to CO_{ads} formation during the ethanol electrooxidation.[15,31] An analogous reasoning can be used here to understand the similar behaviour observed during GEOR: at high potentials, the CO produced is readily consumed yielding CO_2, while at potentials lower than 0.5 V the oxidation rate of adsorbed CO is decreased since the formation of oxygen containing species (OH_{ads}) on the surface, necessary to consume the CO_{ads}, is potential-dependent.[15] At potentials lower than 0.4 V the formation of OH_{ads} from water is disfavoured leading to a surface blocked by CO and other strong adsorbed intermediates. The GEOR is resumed on the positive scan at different rates since water adsorption and OH formation need free surface sites to occur. However, species that built up on the surface at lower potentials should be displaced or consumed to release those sites, which leads to reactivation for GEOR.

In addition, in the negative-going potential scan, the CV profile of the reactivation wave also depends on the density of defects on the surface. Electrodes containing a predominant influence of the (111) sites present very complex and broad peaks, the intensity of which increases continuously along cycling. On the other hand, the most disturbed surfaces show an intense peak that slightly diminishes during cycling.

3.3 FTIR *in situ* experiments

Fig. 3 shows spectra obtained with Pt(111), Pt(111)-20 and Pt(111)-80. The main band assignments are similar to those

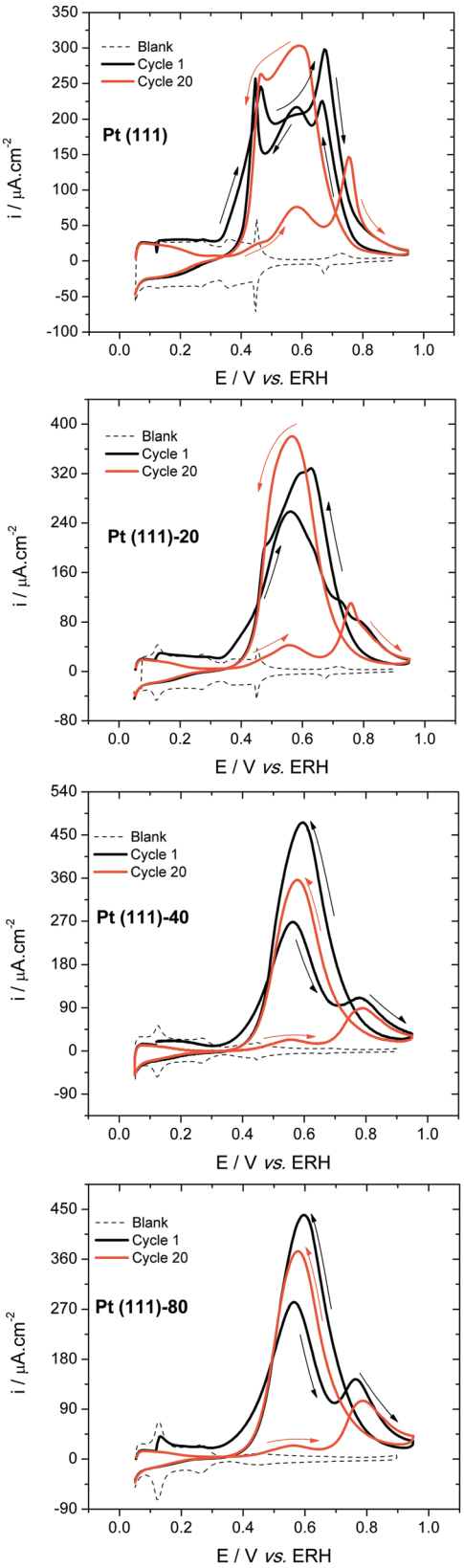

Fig. 2 Cyclic voltammograms obtained in 0.2 M GlOH and 0.5 M H_2SO_4 solution with Pt(111), Pt(111)-20, Pt(111)-40 and Pt(111)-80. v = 0.05 V s^{-1}. The arrows indicate the direction of the scanning.

 This journal is © the Owner Societies 2016

Published on 16 August 2016. Downloaded by UNIVERSIDAD SAO PAULO on 21/10/2016 16:36:44.

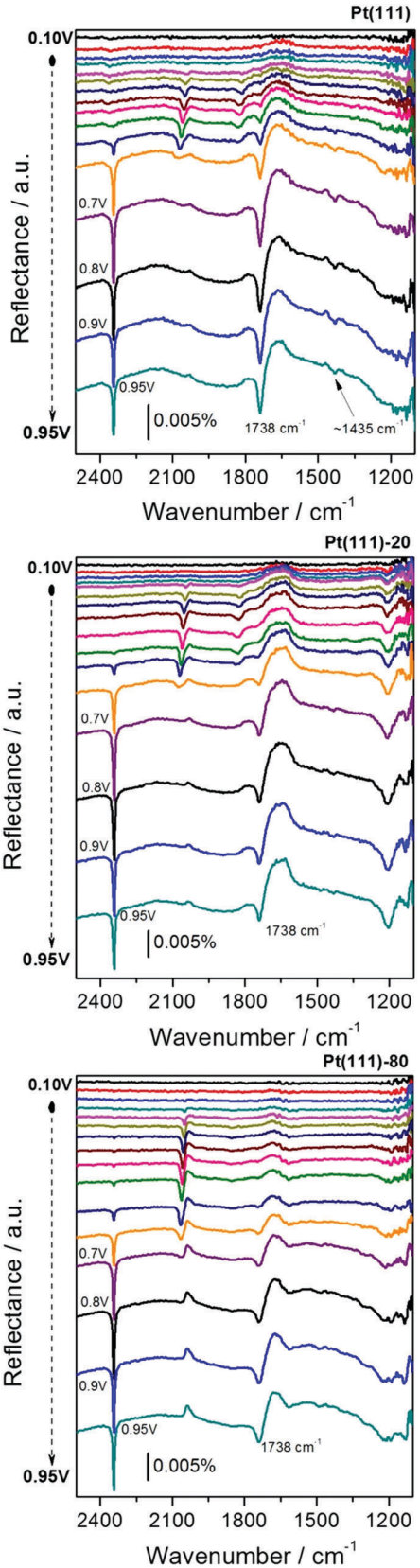

Fig. 3 FTIR spectra obtained in 0.2 M GlOH and 0.5 M H_2SO_4 solution with Pt(111), Pt(111)-20, and Pt(111)-80. With the three surfaces we can follow the working electrode potential dependence of the CO, CO_2 and C═O bands. Spectra at 0.75 V and 0.85 V are not present for the sake of clarity.

observed in our previous work about Pt(100).[13] Briefly, for all the electrodes, we observe: (i) a band centered at 2343 cm^{-1} corresponding to the asymmetric stretching of CO_2; (ii) two bands, the vibration frequency of which changes with the electrode potential, corresponding to on-top and bridge bonded CO, located around 2040–2050 cm^{-1} and ~1830 cm^{-1}, respectively; (iii) a band centered at approximately 1738 cm^{-1} corresponding to a carbonyl containing compound (C═O). Due to the superimposition of several bands we will not pay attention to the region between 1100 and 1300 cm^{-1} despite the fact that SO_4^{-2}, HSO_4^-, GlOH and some possible oxidation products present features in this region.

In order to establish an eventual relationship between the formation of intermediates and products and the electrochemical results, we integrate the areas of CO_2 and CO bands. The broad band at ~1640 cm^{-1} is due to the entrance and the exit of water from the thin layer. This band hampers the integration of the band corresponding to C═O groups. Hence, in an attempt to follow the development of this band along the potential scanning we measured the band height instead of trying to determine its area. The data corresponding to four signals are shown in Fig. 4.

In Fig. 4 we can see two regions, the first one takes place at $E <$ ~0.55 V, where only CO bands are detected. For Pt(111) this band is generated only by the production of CO as a consequence of the GlOH dissociative adsorption. On the other hand, the defected surfaces present on-top CO negative bands (see Fig. S4, ESI†), the intensity of which increases with the defect density, indicating that some of the CO bands appearing in the low potential region correspond to CO already present at the beginning of the experiment. Between 0.55 and 0.65 V the CO band completely disappears due to its oxidation to CO_2, probably the most observed reaction pathway for the electrooxidation of small organic molecules in acidic media. Consequently, in the same potential domain, there is a sudden increase of the CO_2 band and other corresponding to a C═O that we will discuss later.

The mere visual inspection of Fig. 3, 4 and Fig. S4 (ESI†) reveals important differences when the surfaces are compared: the relative intensity of the C═O band decreases significantly

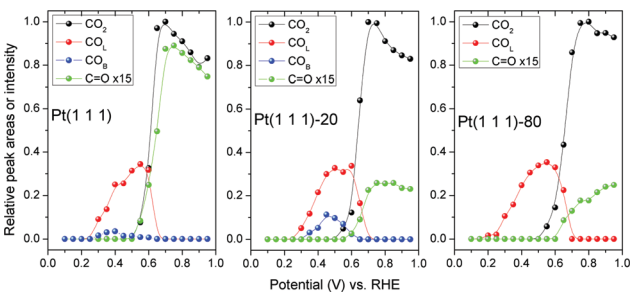

Fig. 4 CO and CO_2 integrated band area and C═O band height of spectra shown in Fig. 3. The relative C═O/CO_2 ratio diminishes markedly when we add defects on Pt(111). The increase of the CO band between 0.20 V and ~0.55 V demonstrates the generation of this molecule on all the surfaces, however, for the electrodes with defects some of the CO were already present at the beginning of the experiment.

Published on 16 August 2016. Downloaded by UNIVERSIDAD SAO PAULO on 21/10/2016 16:36:44.

as the surface is disturbed. It is important to note that this result seems to be opposite to that found with Pt(100)[10] where the C=O band increases as the surface is disturbed. However, the work of Garcia *et al.* showed that GlOH is selectively oxidized to glyceraldehyde (Gld) (which is easily oxidized to GA) on Pt(100).[10] Thus, the C=O band that increases as we add defects on Pt(100) is likely due to an increase in the production of GA. Our present results suggest that defects induce different pathways for Pt(111), as will be discussed later.

It is well-known that the GEOR can generate several products with added value.[6,7,10] In order to identify our main product we recorded FTIR spectra of some of the most probable GlOH oxidation products (Fig. S5, ESI†). We determine that Gld does not have any important feature between 1200 and 3000 cm^{-1}, which makes it impossible to follow its formation by FTIR. On the other hand, dihydroxyacetone (DHA), GA, glycolic acid (GCA), glyoxylic acid (GOA), mesoxalic acid (MOA) and tartronic acid (TA) show at least one intense band centered between 1725 and 1740 cm^{-1}.

TA and MOA also have important features at 1620 and 1640 cm^{-1}, respectively, which do not seem to be present in our spectra, even when the water band is small. The presence of the band of the water could clearly mask the presence of weak bands of these compounds. GOA, DHA, GCA, GA and FA present intense bands between 1730 and 1740 cm^{-1}, which suggests that in principle all of them could be the species responsible for the C=O vibrations in the present case. If we look carefully at the region around 1435 cm^{-1} in the spectra obtained with Pt(111), that is, with the surface that produces the most intense C=O feature, we can detect the presence of a small but clear band in this domain. Coming back again to Fig. S4 (ESI†), we can see that the two main bands of DHA match very well with those observed for Pt(111) at 1738 and 1435 cm^{-1}, which is in line with the results of Garcia *et al.*

Our results, supported by those of Garcia *et al.*[10] (even considering the differences in the experimental conditions), strongly suggest the production of DHA (which is an interesting high-value oxidation product of the GEOR[5]). Hence, this compound seems to be responsible for the C=O band that we analysed in the previous paragraph.

Although the production of DHA (which is an interesting high-value oxidation product of the GEOR[5]) in our experiments is likely, we will need other techniques than FTIR to confirm the result, mainly because we have not analysed all the possible GlOH oxidation products. Besides that, the use of techniques, such as HPLC, would help to follow the Gld production, which is not possible with FTIR.

It is important to note that in the spectra taken with the modified surfaces, the band at 1435 cm^{-1} could not be seen. However, this is not an indication that the main band belongs to a different product other than that observed with the ordered surface. It seems more likely that the band at lower wavelength simply cannot be seen, once it is markedly less intense than the C=O band. Considering that both bands seem to be related to DHA, when we used disordered surfaces, the production of DHA is inhibited and both signals diminish accordingly, which turns the smaller one indiscernible.

Summarizing, we find a different trend in the C=O/CO_2 ratio using Pt(100) in our previous work[13] and in this one with Pt(111). For Pt(100) the C=O band increases with the defect density, which is very likely due to an increase in the production of GA. In this work we observed the most intense C=O band for the well-ordered Pt(111) surface. Interestingly, in the present case this band seems to be due to the production of DHA, which is hindered by the presence of defects and justifies the decrease of C=O signals as the (111) surface becomes more disturbed.

Fig. 4 clearly shows different events in two potential domains as we discussed before. In line with it, the CV forward scan shows two well discernible oxidation features. The FTIR results permit us to conclude that the first voltammetric oxidation peak is connected to the GlOH oxidation to form CO. Besides, the second peak, which is more intense and has a much bigger charge, can be related to the production of CO_2 and species containing C=O groups. Both CO_2 and CO bands change sharply (increasing and decreasing, respectively) at the same potential. After that, the CO_2 band decreases monotonously, due to the diffusion of the molecules out of the thin layer. It indicates that the CO_2 is mainly produced due to the oxidation of the CO formed at lower potentials. Thus, at high potentials, the currents measured after the CO_2 oxidation should probably only come from the GlOH oxidation to C=O. This result is totally different from what we found with Pt(100) surfaces, the CO_2/CO ratios of which are at least 20 times larger than those we measured for Pt(111).[13]

These results may also permit us to understand why the first oxidation peak of the stable CVg continuously decreases as the surface defect density increases. We conclude before that the charge of this peak is related to the GlOH dissociative adsorption to form CO. Even though the relative quantities of CO are comparable for all the surfaces, the CO_2/CO that is observed in the scan (discounting what we already had at the beginning of the cycle) augments with the surface defect density.

3.4 Density functional theory calculations

To support and complement our electrochemical and spectroelectrochemical results, we performed DFT investigations of the complex structure consisting of water, GlOH and CO molecules on a defected Pt surface. This permits us to understand how the defects on a Pt(111) surface influence the interaction of the molecules with the catalyst, which can help to provide a picture of the GEOR.

Our DFT calculations were designed to obtain a description of key points, which can help to provide a complete picture of the GEOR. Moreover, our surface model includes the effects due to the interaction of molecules with low-coordinate sites, which is a key point to the interactions.

The lowest energy structures for the systems studied here are shown in Fig. 5 and 6, while their structural parameters compared with gas phase molecules, the distance between molecules and surfaces, and the molecule orientation are listed in Tables S1–S4 (ESI†). Their higher energy isomers along with the relative total energy are given in Fig. S6–S12 (ESI†).

 This journal is © the Owner Societies 2016

Published on 16 August 2016. Downloaded by UNIVERSIDAD SAO PAULO on 21/10/2016 16:36:44.

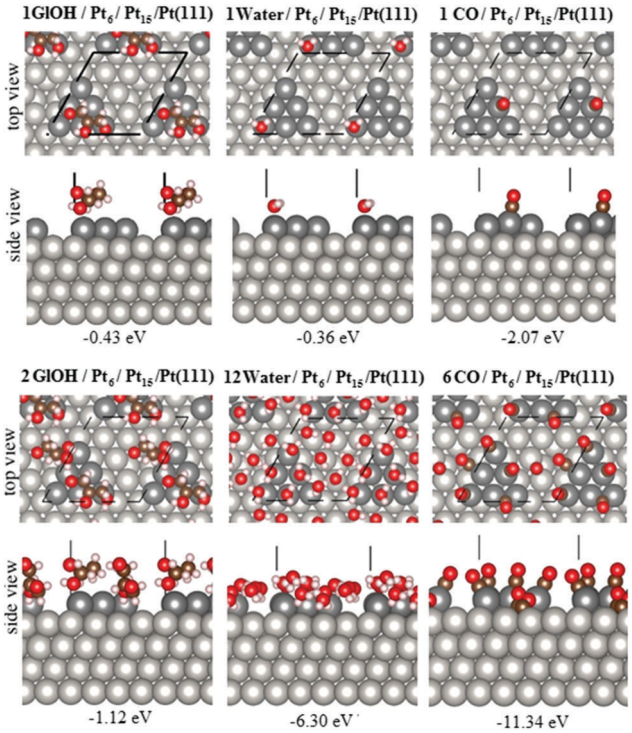

Fig. 5 The lowest energy configurations of 1 GlOH, 1 water, 1 CO, 2 GlOH, 12 water and 6 CO molecules on $Pt_6/Pt_{15}/Pt(111)$. The numbers below correspond to the adsorption energy. The single GlOH, water and CO molecules bind on the P_6 defect sites. Both the GlOH molecules bind to the on-top Pt_6 defect sites linked through H bonds. All the 12 water molecules are on the surface, forming H binds. In the 6 CO molecules, 5 configurations are bonded to the surface defect and the remaining one is on the terrace.

Table 1 presents the energetic properties of the lowest energy structures, such as the adsorption energy, E_{ad}, and the work function change, $\Delta\Phi$, obtained by standard PBE and vdW corrected PBE approaches.

3.5 Adsorption of 1 GlOH, 1 water and 1 CO molecules on $Pt_6/Pt_{15}/Pt(111)$

We found that one GlOH, water and CO molecules bind on the P_6 defect sites (Fig. 5), with the O–Pt bond lengths of 2.30 and 2.33 Å, respectively, and the C–Pt bond length of 1.84 Å, where GlOH and water are nearly parallel to the surface, which is consistent with previous calculations for plain Pt surfaces.[32,33] In the configurations in which GlOH, water and CO are on the terrace (see Fig. S6, S8 and S10, ESI†), their relative total energies increase by 0.43, 0.21 and 0.57 eV, respectively. Additionally, the binding of the molecules with the vacant Pt site does not lead to the increase of the stability of the system, *e.g.* such configurations are higher in energy than the lowest energy structure by 0.43, 0.19 and 0.70 eV, respectively. Thus, there is a strong preference for binding of molecules on lower coordinated Pt sites.

Upon adsorption, GlOH undergoes slight changes in its structure. More detailed information about the molecule structural changes can be seen in Table S1 (ESI†). As supported by our previous work,[32] the adsorption strength is 0.07 eV larger for 1 GlOH than for 1 water. In contrast the CO molecule binds 4.8 times much stronger than GlOH, due to its chemisorption nature.

3.6 Adsorption of 2 GlOH and 12 water molecules on $Pt_6/Pt_{15}/Pt(111)$

For 2 GlOH molecules we found that both molecules bind to the on-top sites of the Pt_6 defect with the smaller O–Pt bond lengths of 2.28 and 2.29 Å (Fig. S7, ESI†). The molecule orientations are different with respect to the surface vertical, *i.e.* β = 52 and 72° linking through H bonds with an O–H bond length of 1.82 Å. Once 1 GlOH moves to the terrace, the energy of the system enhances by 0.28 eV.

The most stable system containing 12 water molecules (Fig. S9, ESI†) presents a structure where all molecules are on the surface, among them 6 molecules bound to Pt_6. All molecules adsorb nearly the on-top site, where 5 water molecules are parallel (O–Pt of 2.28–2.33 Å), while others are down-right to the Pt surface (O–Pt = 3.30–4.01 Å). The molecule located over the vacancy is also down-right oriented. Water molecules form H bonds between them with an O–H bond of 1.66–2.04 Å. In the higher energy structure all molecules are located over the defects, *i.e.* 6 water molecules bind with Pt_6, and all of them create H bonds. The energy increases by 0.47 eV for this configuration, while the structure in which only 1 water molecule is attached to the surface has much higher energy, *i.e.* 1.78 eV more than the lowest energy structure. That is because the molecule–surface interaction highly contributes to the total energy of the system. Thus, a few GlOH and water molecules on the defected Pt surface favour binding with the surface, particularly with the Pt_6 defects, linked by H bonds.

It is important to note that the adsorption energies per molecule increase with the increasing number of molecules on the surface, *e.g.* for 1 GlOH and 2 GlOH molecules the adsorption energies are −0.43 and −1.12 eV, while for the 2 separate molecules the adsorption energy could be only −0.86 eV. This difference can be explained by the contribution of H bonding to the adsorption energy of 2 GlOH molecules. The same is valid for water molecules.

3.7 Adsorption of 6 CO molecules on $Pt_6/Pt_{15}/Pt(111)$

For 6 CO molecules on the surface the most favourable configuration is the one with 5 CO (4 on-top and 1 bridge) molecules bonded to the surface defect and 1 CO molecule on the bridge site, and on the terrace (Fig. S11, ESI†). The C–Pt bonds are 1.85–1.86 Å on the on-top and 2.00–2.13 Å on the bridge sites. This configuration is preferred because of the well-known stronger binding of CO molecules with under-coordinated atoms, while in the case in which all the CO molecules are on the Pt_6 defects, the structure had a strong problem with convergence because of the increased intermolecular repulsions. Finally, when we move 2 molecules from the defect to terrace sites, the energy of the system enhances by 0.25 eV. The minimum distance between the molecules is 3.70 Å. Thus, the Pt_6 defects play an important role in providing stronger binding with CO molecules.

Published on 16 August 2016. Downloaded by UNIVERSIDAD SAO PAULO on 21/10/2016 16:36:44.

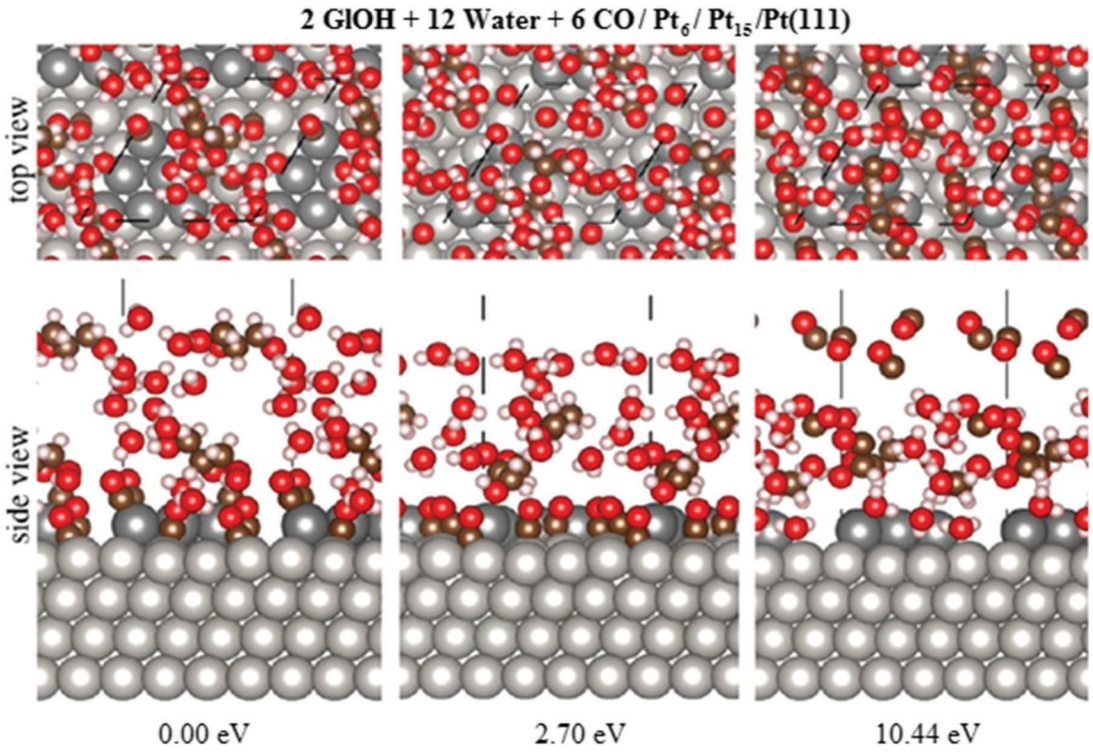

Fig. 6 The lowest and higher energy configurations of 2 Gly + 12 water + 6 CO on $Pt_6/Pt_{15}/Pt(111)$. The numbers below correspond to the relative total energy. In the lowest energy structure CO molecules bind directly to the Pt surface, 3 of them to the low coordinated Pt defects, while most of the water and GlOH molecules are far from the surface forming H bonds. The structure in which water and GlOH bind to the surface and CO molecules are far from the surface is more than 10 eV higher in energy.

Table 1 Energetic properties of the lowest energy structures, such as adsorption energy, E_{ad}, and work function change, $\Delta\Phi$, obtained by standard PBE and vdW corrected PBE approaches

Structure	E_{ad} (eV)	E_{ad}^{vdW} (eV)	$\Delta\Phi/\Delta\Phi^{vdW}$ (eV)
1 GlOH/Pt	−0.43	−0.91	−1.07/−1.02
2 GlOH/Pt	−1.12	−2.45	−1.29/−1.26
1 water/Pt	−0.36	−0.46	−1.04/−1.27
12 water/Pt	−6.30	−9.26	−1.42/−1.37
1 CO/Pt	−2.07	−2.25	−0.18/−0.40
6 CO/Pt	−11.34	−12.91	0.24/0.22
2 GlOH + 12 water + 6 CO/Pt	−23.89	−26.62	−1.78/−1.04

We found an opposite behaviour of the total adsorption energy with the increasing number of CO molecules compared with GlOH and water adsorption. For example, the total adsorption energy increases from 2.07 to 11.34 eV for 1 CO to 6 CO molecules, respectively, decreasing the adsorption energy per molecule, *i.e.* from 2.07 to 1.89 eV per CO molecule, which can be explained by the increased repulsion between CO molecules.

3.8 Adsorption of 2 GlOH, 12 water and 6 CO molecules on $Pt_6/Pt_{15}/Pt(111)$

In the lowest energy structure of the high coverage mixture of GlOH, water and CO molecules (Fig. 6 and Fig. S12, ESI†), we found that all the CO molecules bind directly to the Pt surface, where 3 of them are on the lower coordinated Pt defects (C–Pt bonds of 1.83–1.85 Å). Moreover, 2 water molecules are also on the defect (O–Pt bonds of 2.16–2.20 Å). The direct binding of all the CO molecules to the surface can be explained by the stronger binding of CO with the Pt surface compared with GlOH and water. The remaining water and GlOH molecules are far from the surface (with O–Pt bond lengths from 5.26 to 12.51 Å). All water and GlOH molecules create H bonds between them. In contrast, the structure, in which 3 water molecules and 1 GlOH bind to the surface and all the CO molecules are far from the surface, is more than 10 eV higher in energy.

For the system of the mixture of the molecules (2 GlOH + 12 water + 6 CO) the total adsorption energy is larger than that for the separated systems, *i.e.* 23.89 eV *vs.* 18.76 eV, respectively, which can be explained by the contributions of the energy of H bonding.

The inclusion of the vdW correction to the total energy calculations results in the slight change in the atomic structure and the enhancement of the adsorption energy of the systems, as expected from our previous works.[32,33] The results of the structural changes and adsorption energies are given in Tables S2–S5 and discussed in the ESI.†

The results of the calculations of the work function and work function changes are also given and discussed in the ESI.†

4 Conclusions

In summary, we found that the presence of defects on Pt(111) single crystals plays a decisive role in the interactions between the adsorbate molecules and the catalyst. Namely, in the lowest

 This journal is © the Owner Societies 2016

Published on 16 August 2016. Downloaded by UNIVERSIDAD SAO PAULO on 21/10/2016 16:36:44.

energy configurations for the GIOH–water–CO mixture supported on Pt surfaces, CO binds directly to the Pt atoms on the surface, while most of the water and GIOH molecules are located farther from the surface and form a network of water–GIOH molecules interconnected by the presence of H bonds. This picture can be explained by the stronger adsorption energy of CO on Pt compared with the water or GIOH molecules, in which the bonds are weaker and dominated by long range van der Waals interactions. To confirm our picture, the opposite configuration, in which water and GIOH bind directly to the Pt substrates while CO is far from the surface, is more than 10 eV higher in terms of energy configurations.

These calculations support our FTIR results and allow us to infer that the CO adsorption/oxidation pathways dominate the GEOR electrochemistry. The fact that CO binds stronger than water and GlOH to almost any Pt surface (also considering the calculations showed in our previous work) permits us to explain why the C═O compounds are generated only after some CO oxidation. When taken together electrochemical and spectroelectrochemical results and DFT calculations suggest that in the stable CVg, all the surfaces are close to a full CO coverage.

The density of defects affects the selectivity of Pt(111) and Pt(100) surfaces in a different manner. Namely, when introduced in Pt(100), the defects increase the relative production of GA, while when introduced on Pt(111) they negatively affect the production of DHA.

Our findings open up the possibility to establish an unequivocal correlation between the density of defects of a given surface and the selectivity of it towards specific end-products, based on the previous adsorption steps. It could in principle be understood by performing DFT studies involving adsorbates with different structures.

References

1 World energy outlook 2015, *International Energy Agency (IEA)*, http://www.worldenergyoutlook.org/.
2 Renewables 2015 Global Status Report, http://www.ren21.net/status-of-renewables/global-status-report/.
3 Y. Kwon, K. Schouten and M. T. M. Koper, *ChemCatChem*, 2011, **3**, 1176–1185.
4 Y. Kwon, J. P. Thomas, M. Hersbach and M. T. M. Koper, *Top. Catal.*, 2014, **57**, 1272–1276.
5 Y. Kwon, Y. Birdja, I. Spanos, P. Rodriguez and M. T. M. Koper, *ACS Catal.*, 2012, **2**, 759–764.
6 C. Coutanceau and S. Baranton, *Wiley Interdiscip. Rev.: Energy Environ.*, 2016, DOI: 10.1002/wene.193.
7 M. Simões, S. Baranton and C. Coutanceau, *ChemSusChem*, 2012, **5**, 2106–2124.
8 J. F. Gomes and G. Tremiliosi-Filho, *Electrocatalysis*, 2011, **2**, 96–105.
9 P. S. Fernández, M. E. Martins and G. A. Camara, *Electrochim. Acta*, 2012, **66**, 180–187.
10 A. C. Garcia, M. J. Kolb, C. van Nierop y Sanchez, J. Vos, Y. Y. Birdja, Y. Kwon, G. Tremiliosi-Filho and M. T. M. Koper, *ACS Catal.*, 2016, **6**, 4491–4500.
11 Y. Holade, C. Morais, K. Servat, T. W. Napporn and K. B. Kokoh, *ACS Catal.*, 2013, **3**, 2403–2411.
12 P. S. Fernández, C. A. Martins, C. A. Angelucci, J. F. Gomes, G. A. Camara, M. E. Martins and G. Tremiliosi-Filho, *ChemElectroChem*, 2015, **2**, 263–268.
13 P. S. Fernández, J. F. Gomes, C. A. Angelucci, P. Tereshchuk, C. A. Martins, G. A. Camara, M. E. Martins, J. L. F. Da Silva and G. Tremiliosi-Filho, *ACS Catal.*, 2015, **5**, 4227–4236.
14 J. F. Gomes, F. B. Castelo de Paula, L. H. S. Gasparotto and G. Tremiliosi-Filho, *Electrochim. Acta*, 2012, **76**, 88–93.
15 C. Buso-Rogero and J. Solla-Gullón, *J. Solid State Electrochem.*, 2016, **20**(4), 1095–1106.
16 R. M. Arán-Ais, E. Herrero and J. M. Feliu, *Electrochem. Commun.*, 2014, **45**, 40–43.
17 P. S. Fernández, C. A. Martins, M. E. Martins and G. A. Camara, *Electrochim. Acta*, 2013, **112**, 686–691.
18 J. Schnaidt, M. Heinen, D. Denot, Z. Jusys and R. J. Behm, *J. Electroanal. Chem.*, 2011, **661**, 250–264.
19 J. P. Perdew, K. Burke and M. Ernzerhof, *Phys. Rev. Lett.*, 1996, **77**, 3865–3868.
20 S. Grimme, J. Antony, S. Ehrlich and H. Krieg, *J. Chem. Phys.*, 2010, **132**, 154104–154119.
21 P. E. Blöchl, *Phys. Rev. B: Condens. Matter Mater. Phys.*, 1994, **50**, 17953–17979.
22 G. Kresse and D. Joubert, *Phys. Rev. B: Condens. Matter Mater. Phys.*, 1999, **59**, 1758–1775.
23 G. Kresse and J. Hafner, *Phys. Rev. B: Condens. Matter Mater. Phys.*, 1993, **48**, 13115–13126.
24 G. Kresse and J. Furthmüller, *Phys. Rev. B: Condens. Matter Mater. Phys.*, 1996, **54**, 11169–11186.
25 A. Björling and J. M. Feliu, *J. Electroanal. Chem.*, 2011, **662**, 17–24.
26 A. M. Gómez-Marín and J. M. Feliu, *Electrochim. Acta*, 2012, **82**, 558–569.
27 M. Wakisaka, S. Asizawa, H. Uchida and M. Watanabe, *Phys. Chem. Chem. Phys.*, 2010, **12**, 4184–4190.
28 J. Clavilier and D. Armand, *J. Electroanal. Chem.*, 1986, **199**(1), 187–200.
29 K. Itaya, S. Sugawara, K. Sashikata and N. Furuya, *J. Vac. Sci. Technol., A*, 1990, **8**, 515–519.
30 B. Conway, *Prog. Surf. Sci.*, 1995, **49**, 331–452.
31 H. Wang, Z. Jusys and R. J. Behm, *J. Phys. Chem. B*, 2004, **108**, 19413–19424.
32 P. Tereshchuk and J. L. F. Da Silva, *J. Phys. Chem. C*, 2014, **118**, 15251–15259.
33 P. Tereshchuk and J. L. F. Da Silva, *J. Phys. Chem. C*, 2012, **116**(46), 24695–24705.